NAL TR-686T

ISSN 0389-4010
UDC 629.735.014.16:
629.7.062.4:
533.69

TECHNICAL REPORT OF NATIONAL AEROSPACE LABORATORY

TR-686T

Aerodynamic Characteristics of the External USB Powered Lift System Using Side Fences for Enhancement of Coanda Flow Attachment

Masataka MAITA, Hirotoshi FUJIEDA
and Shigemi SHINDO

October 1981

NATIONAL AEROSPACE LABORATORY

CHŌFU, TOKYO, JAPAN

Aerodynamic Characteristics of the External USB Powered Lift System Using Side Fences for Enhancement of Coanda Flow Attachment

Masataka Maita* Hirotoshi Fujieda**, Shigemi Shindo*

ABSTRACT

The fundamental aspects concerning the effect of side fences on powered lift augmentation for the external upper surface blowing propulsive-lift configuration, as ascertained by wind tunnel experiment, are presented in this paper.

From the comparisons of aerodynamic performances we have made of configurations using side fences and of those using either vortex generators or using no special devices, we conclude that the USB propulsive-lift concept using side fences for enhancement of engine exhaust flow attachment has promising potential for attaining very high and efficient powered lift performances.

概　　要

USB方式STOL機の高揚力システムに於いては，低速STOL 性能に要求される高揚力を得るため，推進用エンジンノズルを大きな縦横比の出口形状にしたり，ノズル上面のキックダウン角を大きくとる等のデザインにして，コアンダ効果を促進させる設計にすることが有利であるが，このような低速領域で適したノズルデザインは一般に巡航時にはナセル抵抗やノズル上面のボートテイル剝離による抗力増加で，巡航性能のペナルティをもたらす。巡航及び離着陸の両形態でのデザイン要求を満足させるために，離着陸時用の付着装置として，米国ボーイング社の開発したボルテックス・ジェネレータ等を付ける対策がとられているが，この方式は，それに因る騒音の発生増加，推力損失及び格納のための機構の複雑さといった問題点が指摘されている。かかる問題点に対処するため，格納を必要とせず又，騒音面での要求をみたし，高揚力の増加をもたらす付着装置として，ボルテックス・ジェネレータ方式に代わる一つの解としてサイドフェンス方式を提案し，その研究開発を行なってきた。本研究に於いては，高揚力システム部分模型に因る基礎スタティック試験及びSTOL実験機の8％スケール半裁模型による風胴試験等から，サイドフェンス方式高揚力システムの空力特性について議論し，その有用性を示した。

NOMENCLATURE

AR_e	Aspect ratio defined as nozzle area A divided by square of nozzle height h, A/h^2.
β_u	The nozzle kickdown angle, angle between horizontal and top surface internal leaving angle, [deg.]
ΔP	Static pressure difference relative to ambient pressure P_o
C_p	Pressure coefficient defined as ΔP divided by jet dynamic pressure at nozzle exit, $\Delta P/0.5\rho U_{jet}^2$

* Noise and Emission Research Group
* VISTOL Aircraft Research Group

OEI(In)	One engine inoperative (Inboard engine out)
OEI(Out)	One engine inoperative (Outboard engine out)
N_1	Simulator-engine's fan rotor speed, [rpm]
F_A	Axial force
F_N	Vertical force
T	Static thrust force based upon engine calibrations with flaps removed, $T = \sqrt{F_N{}^2 + F_A{}^2}$
δ_f	USB flap deflection angle, [deg.]
δ_j	Jet turning angle, [deg.]
η_j	Jet turning efficiency
α	Angle of attack, [deg.]
q	Free stream dynamic pressure, $0.5\rho U_\infty^2$
S	Wing area
$\bar{c}$	Mean aerodynamic chord of wing
C_L	Lift coefficient defined as lift force divided by free stream dynamic pressure times wing area, Lift/qS
C_D	Drag coefficient defined as drag force divided by qS
C_M	Pitching moment coefficient defined as pitching moment divided by $qS\bar{c}$
C_j	Thrust coefficient defined as engine thrust T divided by qS
γ	Flight path angle, [deg.]
C_{Lmax}	Maximum lift coefficient

INTRODUCTION

The design of a short takeoff and landing [STOL] aircraft requires high values of maximum lift with appropriate lift/drag ratios. External upper surface blowing is one of the primary concepts for producing the powered high lift required for STOL operations. Powered lift augmentation during low speed STOL operations is derived by deflecting the turbofan engine exhaust flow downward adjacent to the wing/flap upper surface by Coanda principles.[3]

One of the difficulties with USB-STOL aircraft relates to the attachment of the engine exhaust flow to the wing and extended USB flap surfaces during low-speed operations.

Some of the important parameters governing jet exhaust turning characteristics are the thickness of wall jet and the radius of curvature of the flap upper surfaces, which are directly dependent

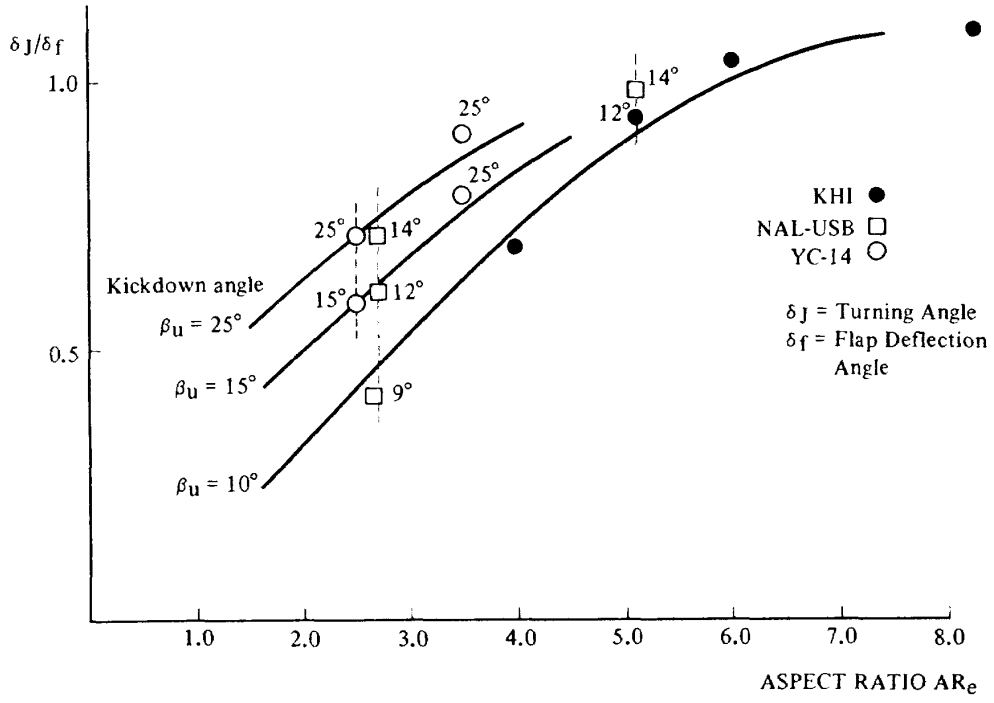

Figure 1 Effects of USB Nozzle Geometries (Nozzle Aspect Ratio, Nozzle Kickdown Angle) on Jet Turning Angle.

upon the USB nozzle wing/flap geometry. The major aerodynamic design efforts in the USB configuration, powered by high-bypass ratio turbofan engines, have been directed to the area of the engine nozzle and the USB flaps.

At low speed, a relatively wide and thin exhaust jet results in better flow attahcment and hence powered lift augmentation, which is usually accomplished by designing the turbofan-engine nozzle exit geometry to have a higher aspect ratio with a higher nozzle kickdown angle. (cf. Figure 1)

In general, optimal USB designs which will enhance the exhaust flow attachment at low speed STOL operations will degrade overall efficiency at a high speed cruise operation. A high aspect ratio nozzle increases nacelle cruise drag and/or high-kickdowned USB nozzle designs will result in cruise drag penelty associated with the nozzle Boattail flow separations[1] as shown in Figures 2 and 3. (cf. Braden et.al.) To overcome the problem of these two incompatible design demands, several flow attachment devices which are retractable during cruise operation have been developed for USB-STOL applications. Vortex generators and USB nozzle side doors on the YC-14[2] are typical examples.

Vortex Generators developed by Boeing Commercial Airplane Co., however, have revealed some defects in their performances. One particular problem is that installation of Vortex Generators resulted in noise increase and thrust losses.[3] Also retractability of 4 Vortex Generators per 1 Turbofan engine during takeoff and cruise operations require several actuator mechanisms which bring in the additional structure complexity and/or weight penalty.

Following the concept of "the simple the better", and to fullfill aeroacoustic design demands that attachment devices should bring about efficient powered lift with aerodynamically cleaner flow deflections[3], we have developed side fences as an alternative solution for enhancing Coanda attachments applied to the USB-STOL propulsive-lift system.[3]

As could be observed in the flow visualization photographs of 1 and 2 (by tufts), mechanisms of enhancing Coanda attachment by side fences

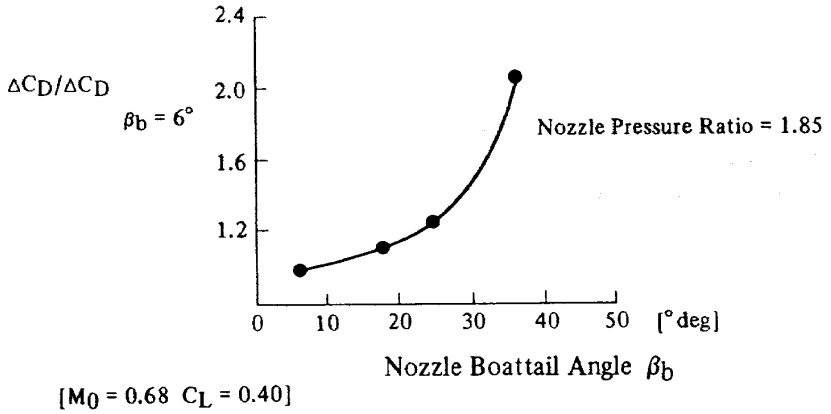

Figure 2 Effect of USB Nozzle Boattail Angle on Nacelle Drag Ratio to $\beta_b = 6°$

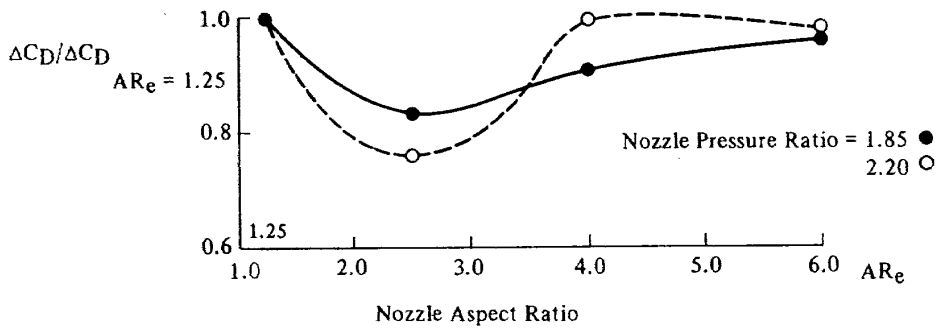

Figure 3 Effect of USB Nozzle Exit Aspect Ratio on Nacelle Drag Ratio to $AR_e = 1.25$

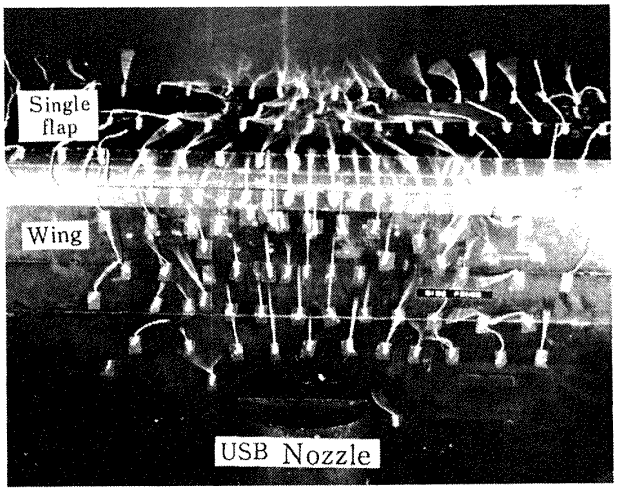

Ambient air flowing in and under the exhaust, causing separations on flap

Flow Visualization Photograph 1
Without any devices

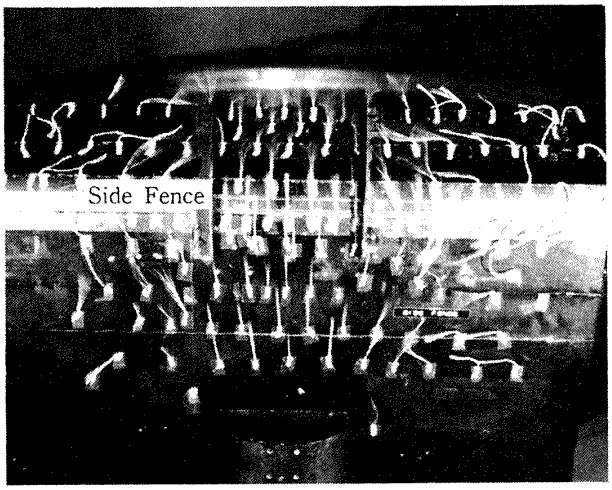

Flow separations on flap being disclosed by Side Fence

Flow Visualization Photograph 2
With Side Fences installed

and vortex generators may be qualitatively compared as follows: the installation of side fences prevents ambient air, which causes exhaust flow separation, from flowing in and under the jet exhaust, while vortex generators, which are installed on wings at an incidence angle of about 30°, prevent it by directing the exhaust flow toward regions where the flow separates to create an outward velocity component. Side fences are installed essentially parallel to the exhaust flow, which results in efficient jet turning without much loss of engine thrust, and does not necessitate retraction during cruise operations which will avoid the additional complexity of USB system structures.

In the present paper, we attempt to summarize the principal results and conclusions concerning the effect of side fences on powered-lift aerodynamic performances as ascertained by wind tunnel experiments, together with preliminary experiments.

PRELIMINARY STUDIES

As preliminary studies, a number of static experiments on the aerodynamic characteristics of side fences have been undertaken. The model assembly used in these preliminary studies was designed by scaling down to exactly 8 percents of the NAL Quiet STOL Aircraft's USB powered

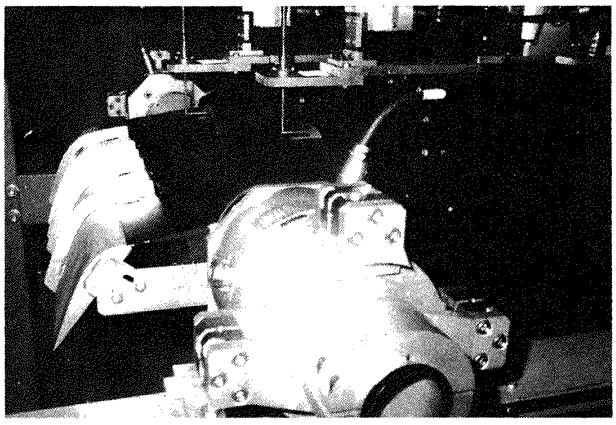

Side View

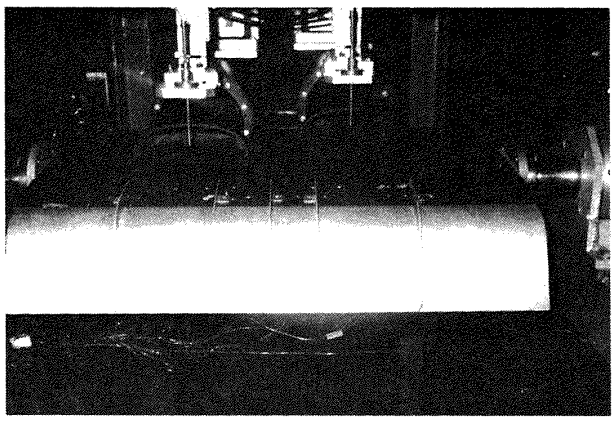

Rear View

Figure 4 Basic Model Configuration used in Preliminary studies

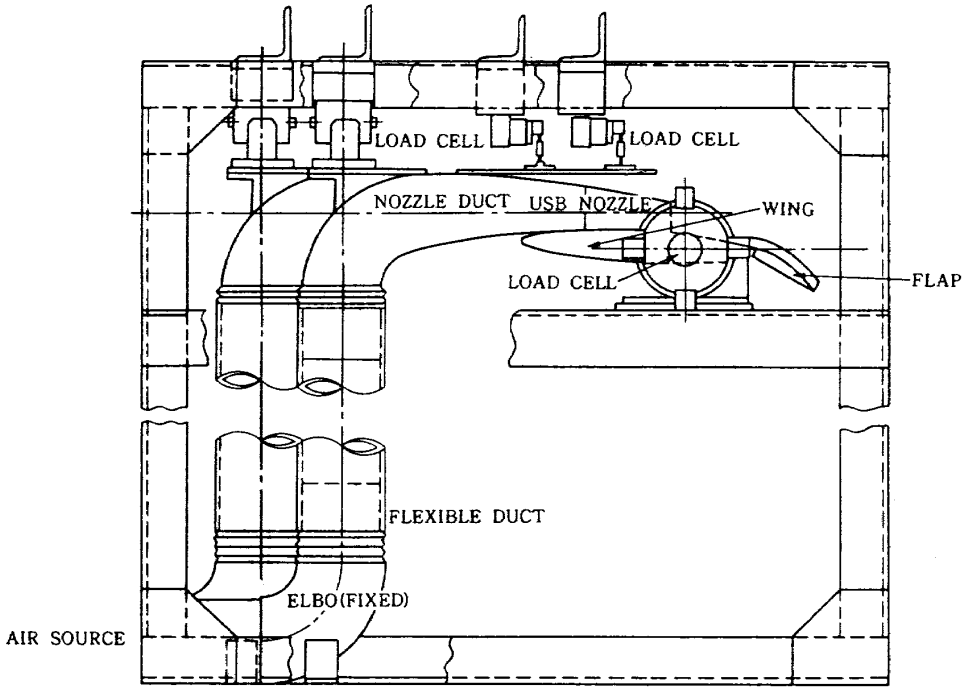

Figure 5 Experimental model setups for preliminary studies

lift system and the turbofan engine exhaust was simulated by a compressed air jet. Photographs of its basic model configuration are shown.

Axial and normal forces exerted by wing and flap, and USB nozzle thrust were measured by 6 Load Cells (cf., Figure 5) from which were then reduced thrust vectoring performances such as the thrust turning angle δ_j and its efficiency η_j. The basic D-shaped USB nozzle exit geometry has an aspect ratio of 2.64 with a kickdown angle of 19° as shown in Figure 6. Some experiments were conducted for cases using different kick-down angle nozzles, i.e., modifications of the basic nozzle β_u=19°, as illustrated by Figures 6 and 7, to compensate for the kickdown effects on Side Fence. Thirty-eight static pressure ports were provided on the main-wing and USB flap upper surfaces and their locations are presented by Figure 8 and 9.

Spanwise static pressure profiles [corresponding pressure ports positions from 21 through 36] are presented in Figure 11, 12, 13 and 14 for the case δ_f=60° configuration, β_u=19° nozzle geometry with different exhaust flow attachment devices, i.e., Side Fences, Vortex Generators and no device respectively. In the figures, the static pressure difference ΔP relative to the ambient P_0

β_u	Δh	ρ
19°	0	∞
22°	1.2	103.9
23.5°	1.9	69.3
26°	2.9	44.6

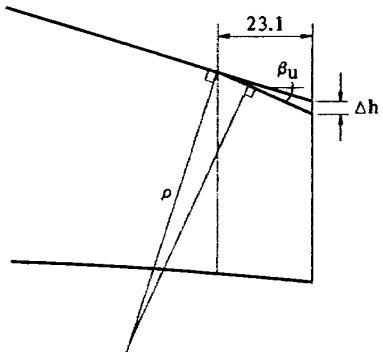

Figure 6 USB Nozzle Geometry
Modifications of a basic nozzle to higher Kickdowned nozzles

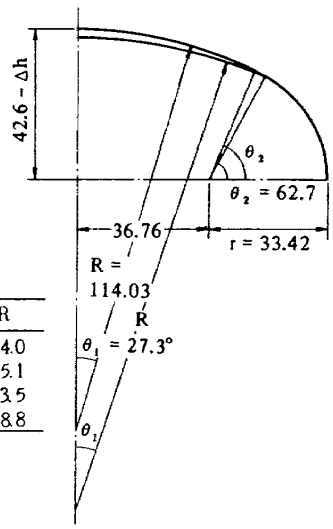

β_u	θ_2	θ_1	r	R
19°	62.7°	27.3°	33.42	114.0
22°	66.2°	23.8°	33.42	125.1
23.5°	68.3°	21.7°	33.42	133.5
26°	71.3°	18.7°	33.42	148.8

Figure 7 USB Nozzle Exit Geometry
Corresponding nozzle exit shapes to Figure 6

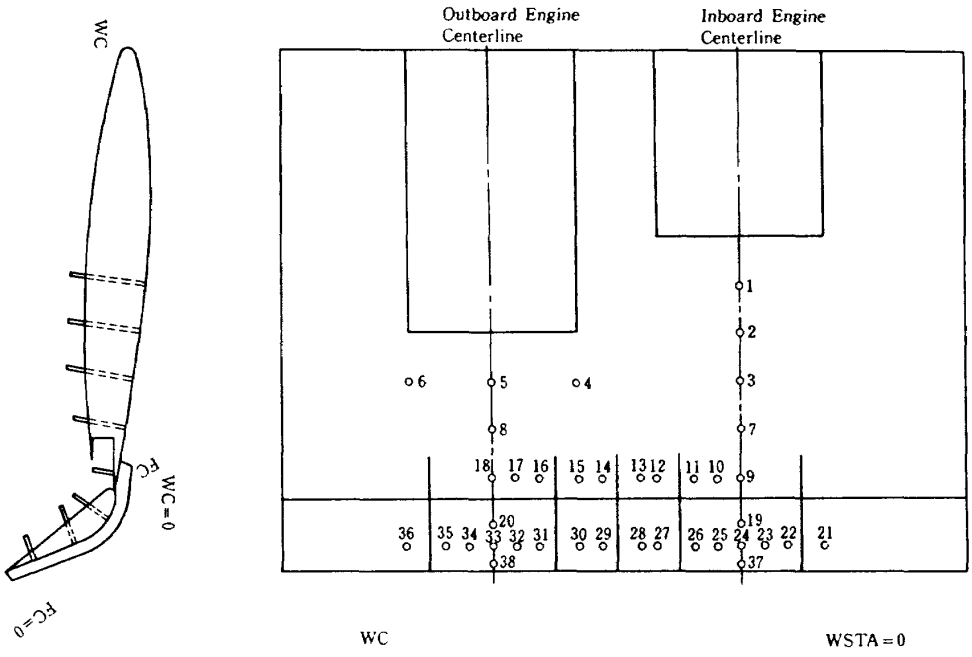

Figure 8 Locations of static pressure ports (38 points) on Wing and Flap upper Surfaces

NO	WSTA	WC	NO	WSTA	FC
1	92.0	187.0	19	92.0	89.0
2	92.0	145.0	20	305.44	98.0
3	92.0	103.0	21	20.0	64.0
4	232.44	103.0	22	52.0	64.0
5	305.44	103.0	23	72.0	64.0
6	378.44	103.0	24	92.0	64.0
7	92.0	61.0	25	112.0	64.0
8	305.44	61.0	26	132.0	64.0
9	92.0	19.0	27	164.8	64.0
10	112.0	19.0	28	178.0	64.0
11	132.0	19.0	29	218.0	64.0
12	164.8	19.0	30	231.2	64.0
13	178.0	19.0	31	265.44	64.0
14	218.0	19.0	32	285.44	64.0
15	231.2	19.0	33	305.44	64.0
16	265.44	19.0	34	325.44	64.0
17	285.44	19.0	35	345.44	64.0
18	305.33	19.0	36	380.04	64.0
			37	92.0	19.0
			38	305.44	19.0

Figure 9 Locations of static pressure ports in terms of Wing Station [WSTA] and Wing and Flap chord [WC, FC]

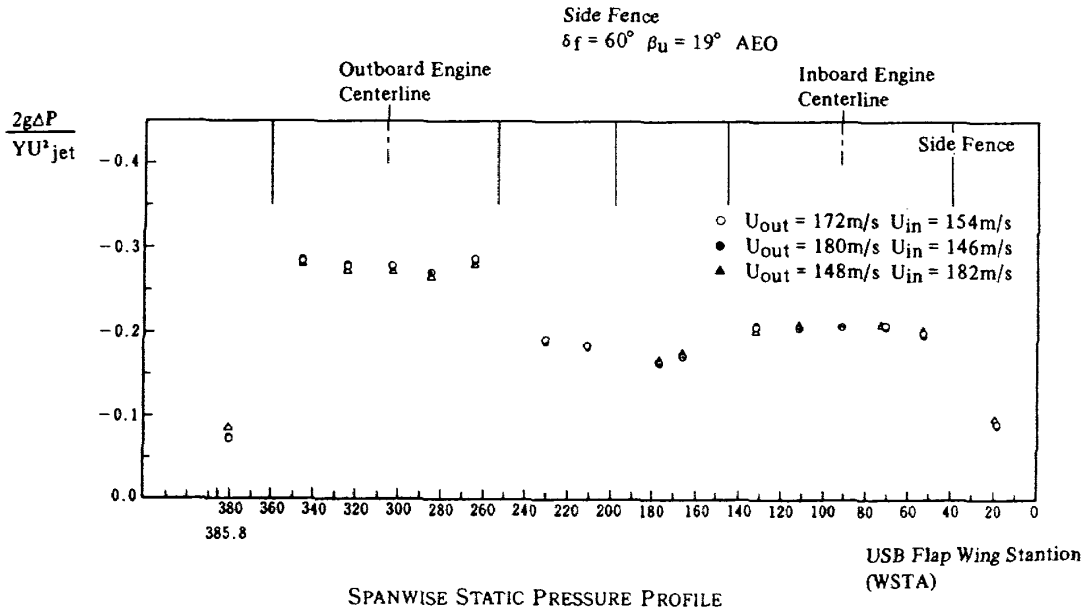

Figure 10 Data comparisons based upon a pressure coefficient C_p by different nozzle set-up velocities, for the same configuration basis.

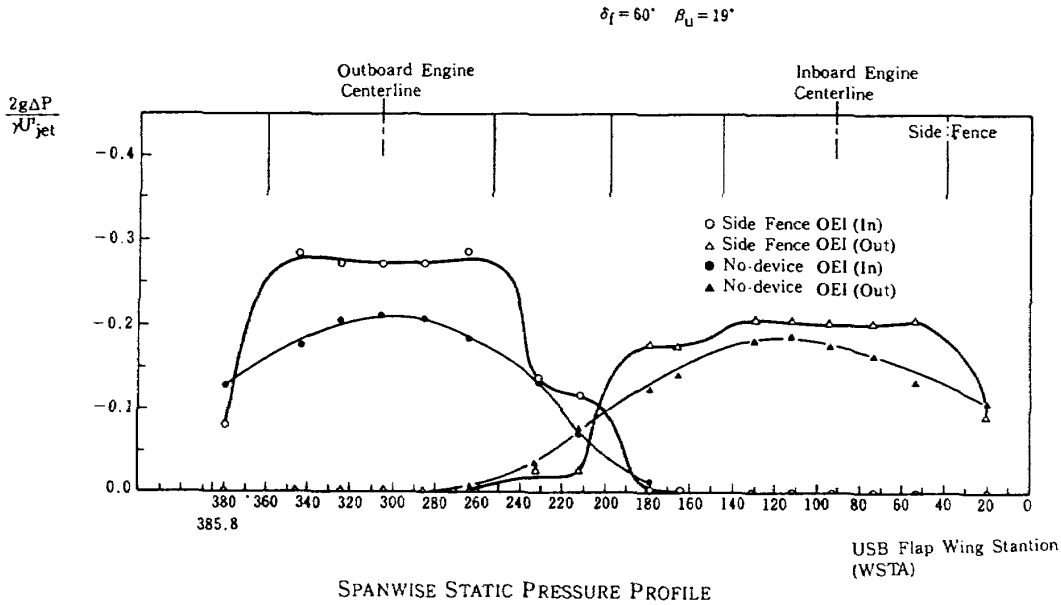

Figure 11 Spanwise C_p profiles of Side Fence (thick solid line) being compared with C_p of no-device case (thin solid line) for one engine operative.

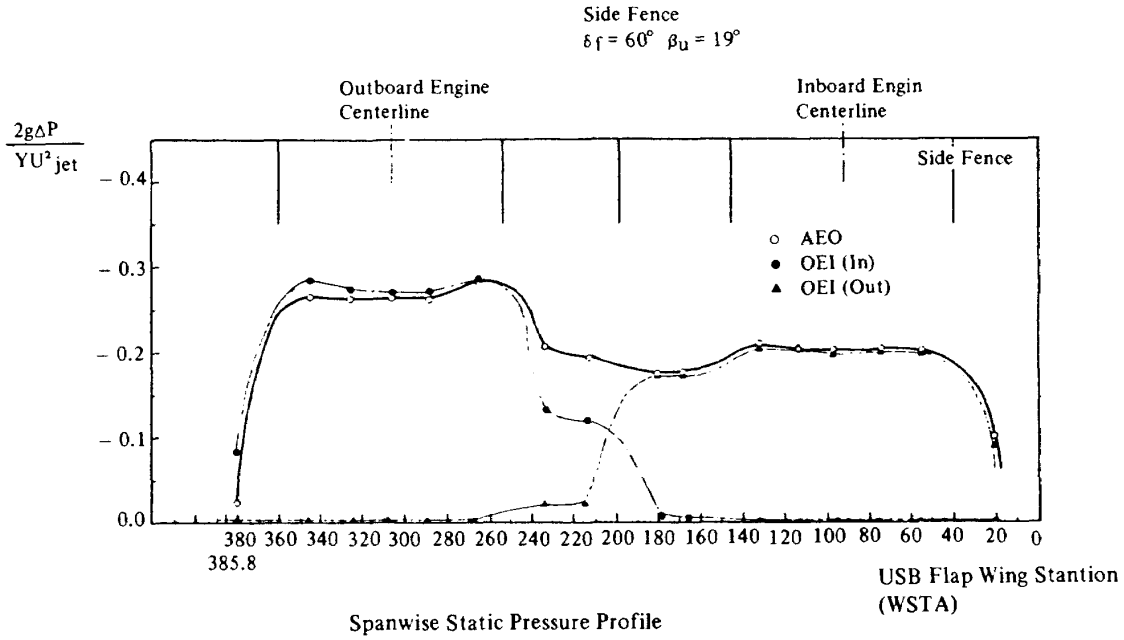

Figure 12 Spanwise C_p profiles of Side Fence case for both engine operative AEO, compared with C_p for one engine operative OEI (In), OEI (out).

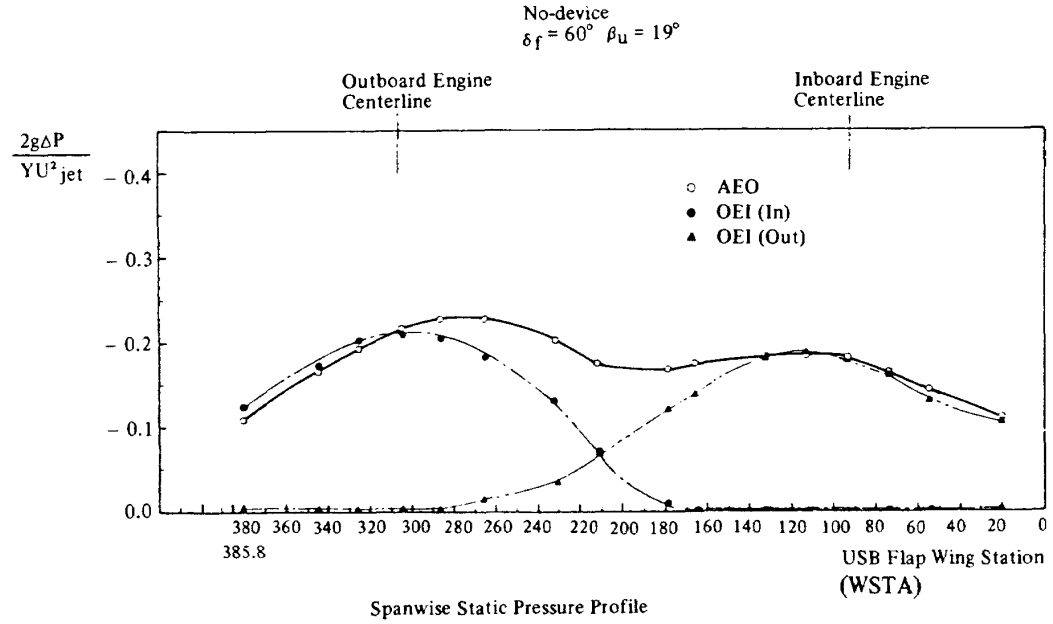

Figure 13 Spanwise C_p profiles of no-device case for both engine operative AEO, compared with C_p for OEI (In), OEI (Out).

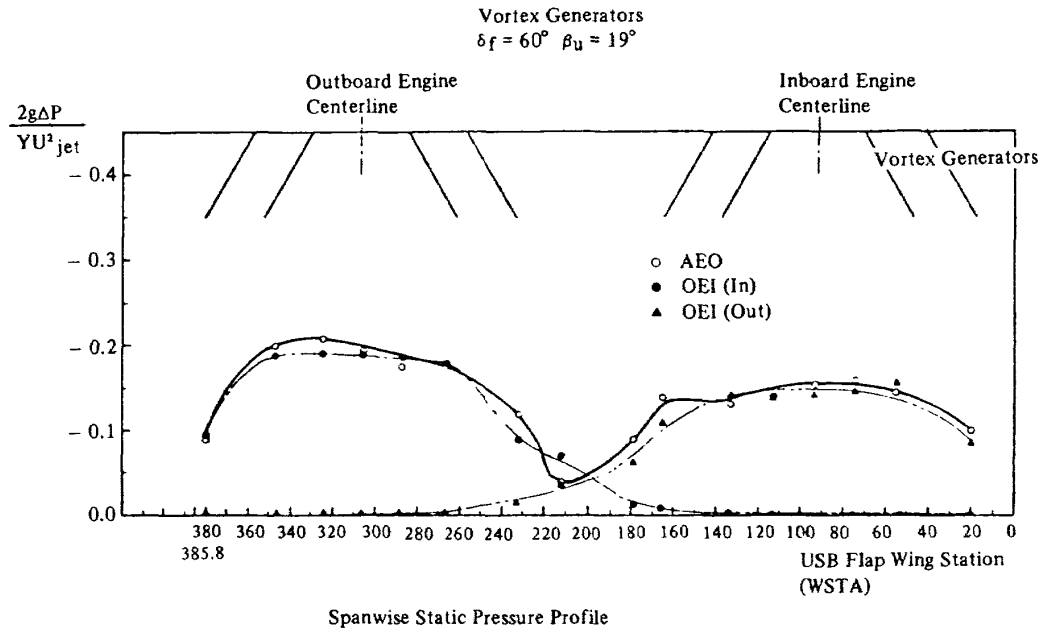

Figure 14 Spanwise C_p profiles of Vortex Generators case for both engine operative case AEO, compared with C_p for OEI (In), OEI (Out).

were nondimensionalized by the nozzle exit dynamic pressure $0.5\rho U^2_{jet}$ as the pressure coefficient C_p. Data comparisons based upon a pressure coefficient C_p avoid the error caused by the nozzle exhaust velocity set-up of each respective case, as shown in Figure 10.

In Figure 11, C_p profiles of Side Fence were compared with those of no-device for one engine operative OEI(In) or OEI(Out). Both engines operative cases [AEO] are represented by thick solid lines in Figures 12 and 13. Side fences produced higher negative C_p profiles compared with no-device or Vortex Generators (cf. Figure 14).

The tendency for two separate low aspect ratio nozzle exhausts from the outboard and inboard engines to appear to combine into a single high aspect ratio nozzle exhaust flow was found except for Vortex Generators, where static pressure recovery occurred in the portions between the two jets [WSTA around 180–240].

Qualitative explanations concerning the roles of Vortex Generators on exhaust flow attachment mechanisms were as follows: i.e. Vortex Generators, installed on wing surface with an incidence angle of 30° or so, directing the exhaust flow toward regions where the flow separates, to create an outward velocity component which then prevents ambient air from flowing in and under the jet exhaust; thinned jet thickness enhancing Coanda attachment; the rotational velocity components of the vortices scrubb boundary layer air from the flap surface [Boundary Layer Control]; Entrainment effect by the inwardly rotating large-scale vortices. One and/or some of the above cited mechanisms were assumed to be caused by Vortex Generators, themselves.

However, as shown in Figure 14, due to thrust losses by Vortex Generators themselves, negative C_p values were reduced and directing exhaust outward by one pair of vortex generators resulted in prevention of the neighbouring vortex generators' role, thus cancelling out the respective neighbouring vortex generators' roles, i.e. for example, outwardly directed exhaust flow by the right-side pair of vortex generators of the outboard engine and the left-side pair of vortex generators of the inboard engine are opposite in direction respectively which thus deteriorates

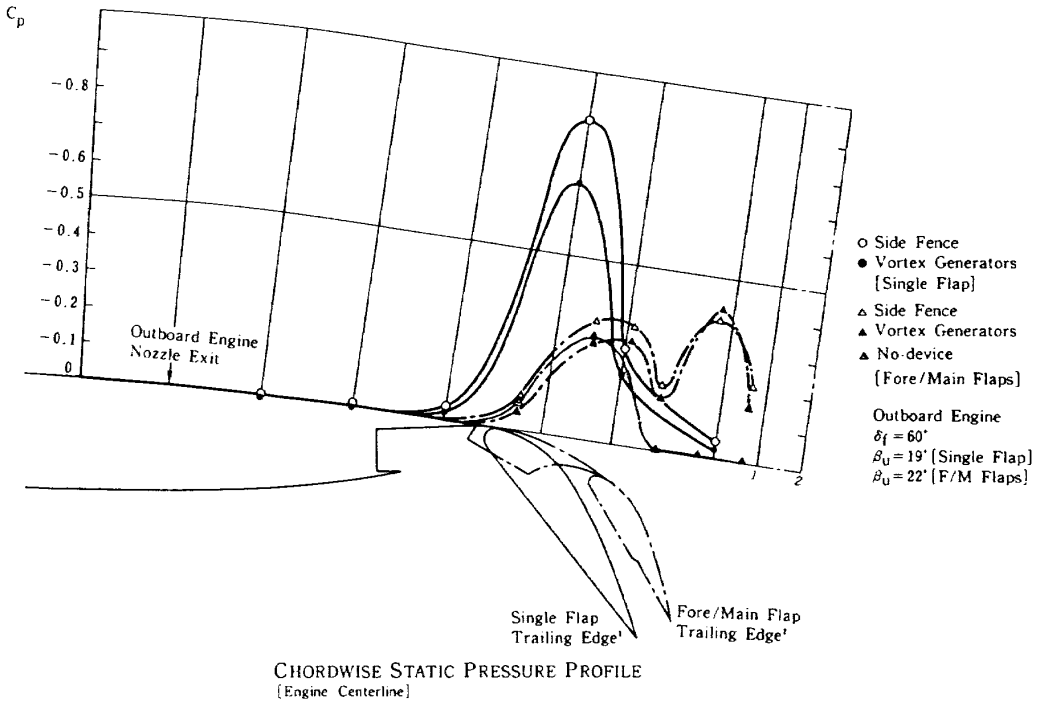

Figure 15 Chordwise C_p profiles outboars engine centerline

both roles as has been found in C_p recovery occurring in the portions near WSTA 180–240.

Chordwise static pressure profiles in terms of a pressure coefficient C_p are presented in Figure 15, comparing Side Fences with Vortex Generators. Solid lines denote C_p profiles along a single flap (δf=60° flap setting) while dotted lines denote profiles along fore and main double flaps (also δf=60° setting; note that the double flap perimetric length over flap upper surfaces is longer and its trailing edge corresponds to the position 2, given in Figure 15). It is of interest to note that a single flap configuration possibly resulted in lesser negative pitching moment than double flap configurations, which eased the longitudinal trim by tail planes, because the aerodynamic center on a single flap (near 1/4 chord) located more forwardly than that attained by double flaps, while lift forces, being proportional to integrals of C_p over surfaces, were approximately equal for the same turning angles δj.

In Figures 16,17,18 and 19, thrust vectoring performances are presented for cases of flap setting δf=60°,55°,40° and 62° respectively where the jet turning angle δj in degrees and the

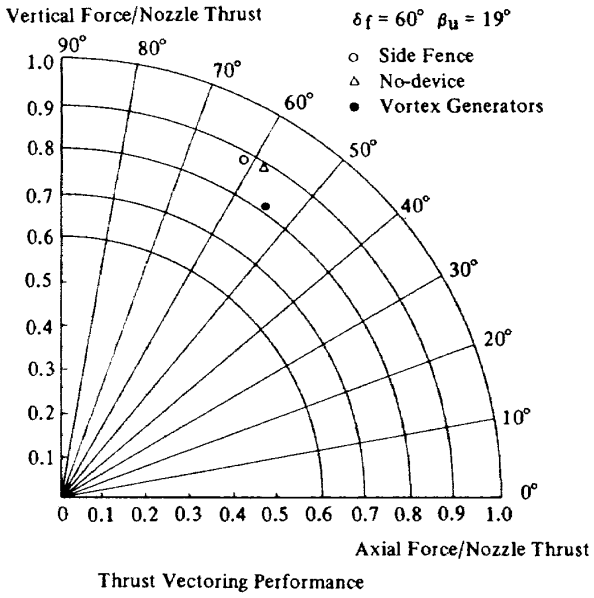

Figure 16 Thrust vectoring performances for flap setting δf = 60°, USB nozzle kickdown angle of 19°.

thrust turning efficiency ηj are expressed in polar coordinates while in Cartesian coordinates, lift force divided by nozzle thrust(y-axis) and drag force divided by nozzle thrust (x-axis). Side fences attained higher turning angles and better efficiencies for all cases compared with Vortex

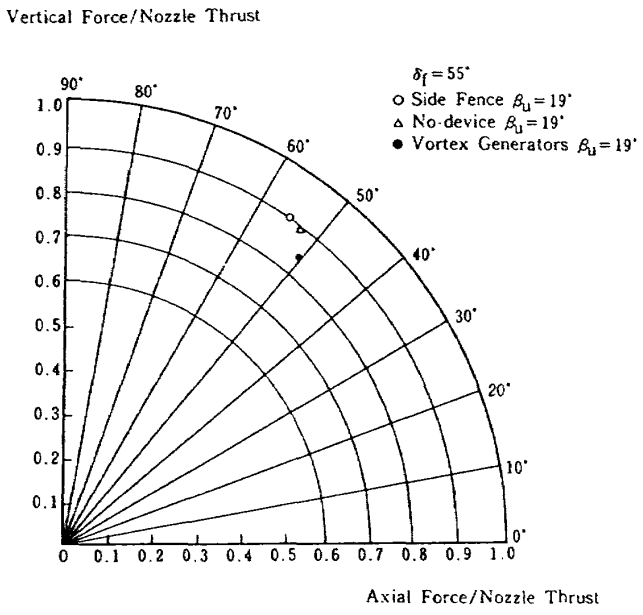

Figure 17 Thrust vectoring performances for flap setting $\delta f = 55°$, USB nozzle kickdown angle of 19°.

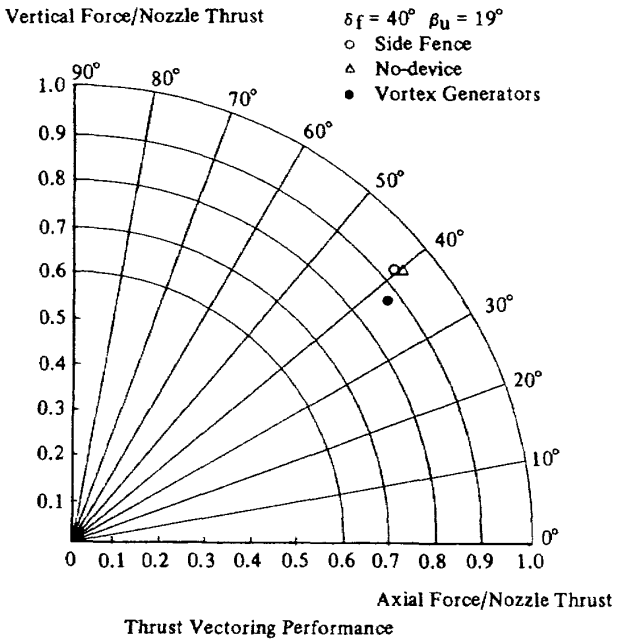

Figure 18 Thrust vectoring performances for flap setting $\delta f = 40°$, USB nozzle kickdown angle of 19°.

Generators as has been suggested by C_p profiles data.

The tendency for the thrust defection without any attachment devices to become comparable to Side Fences for lower flap setting configuration δf=40° was due to an increase in radius of

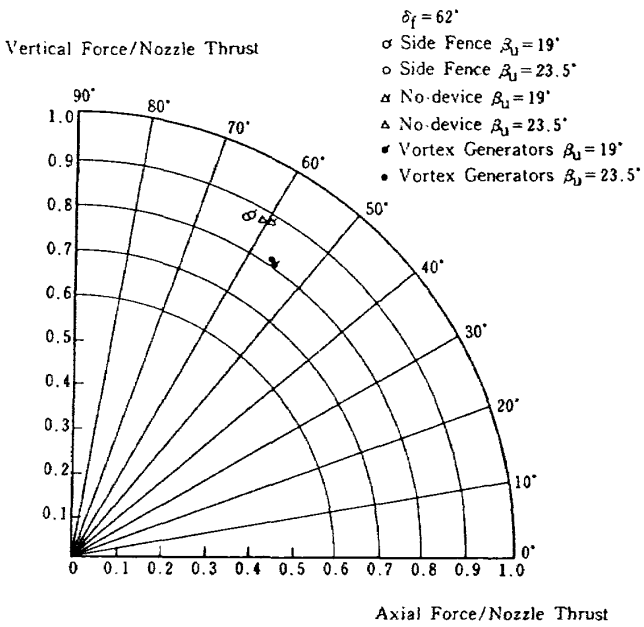

Figure 19 Thrust vectoring performances for flap setting $\delta f = 62°$, USB nozzle kickdown angles $\beta u = 19°$ and 23.5°.

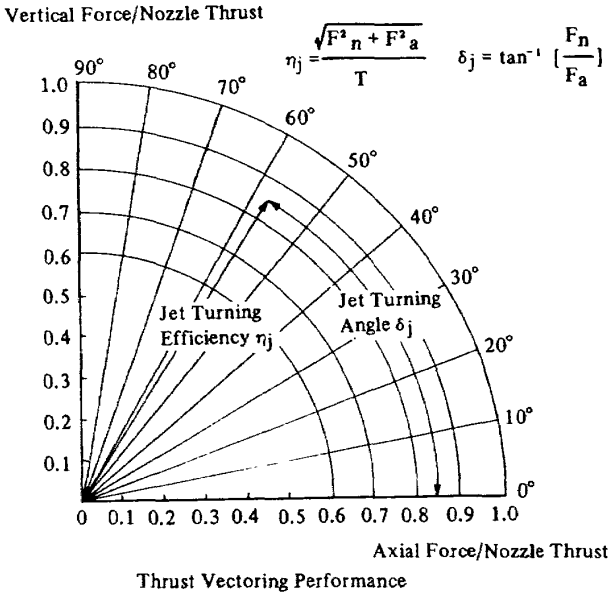

Figure 20 Thrust vectoring performance (jet turning angle δj in degrees and the efficiency ηj being expressed in polar coordinate, lift force (y-axis) and drag force (x-axix), both divided by nozzle thrust being expressed in Cartesian coordinate.

curvature of wing/flap upper surfaces which thus enhanced a Coanda effect by itself and made side fences no longer necessary. Figure 21 presents the effect of inboard and outboard engines thrust ratio X on thrust deflections. The Inboard engine being located farther forward in chordwise than the outboard engine due to a swept back main wing, its exhaust produces higher scrubbing drag over longer flow path lengths as shown in Figure 22. When X takes a value greater than unity (i.e. inboard engine thrust being greater than outboard engine thrust), the turning efficiency η_j tends to deteriorate. However, the jet turning angle δ_j tends to be improved which is thought to be the adjustment effect of the two jets' velocities (the flow path lengths of the inboard side exhaust jet are longer by approximately 2h, where h is the USB nozzle exit height length, and hence its velocity is under more a decayed stage than the outboard jet's) in view of the basic concept that two separate low aspect ratio nozzle exhausts appear to act as a combined single higher aspect ratio nozzle exhaust which enhances the Coanda effect.

By sensing static pressure ports on the Side Fence as shown in Figure 23, C_p profiles were investigated. Figure 24 presents C_p profiles and their contours on a side fence for the flap setting δ_f=60° configuration with the nozzle kickdown angle β_u=19°. Results were of great importance in determining the optimum geometry of side fence. Higher negative values of C_p occurred in the vicinity of small radius of curvature portions indicating that the side fence plays its dominant role there. It might be possible to reduce the heights of side fence near flap trailing edges or wing trailing edges as suggested by the lower negative values of C_p. And also the necessary heights of the side fence depend upon the USB nozzle kickdown angle β_u. Where β_u=26° (cf. Figure 25) corresponding C_p contours shifted to

Kickdown Angle β_u	AEO D_s	OEI (In) D_s	OEI (Out) D_s
19°	3.79	2.89	3.81
23.5°	4.22	3.22	4.27
26°	4.44		
19°	12.19 With Vortex Generators		

AEO All Engines Operative
D_s Scrubbing Drag to Jet Thrust at 26.1kg
OEI (In) Inboard Engine Inoperative
D_s Scrubbing Drag to Jet Thrust at 13kg
OEI(Out) Outboard Engine Inoperative
D_s Scrubbing Drag to Jet Thrust at 13kg

Figure 22 Scrubbing drag over wing surfaces

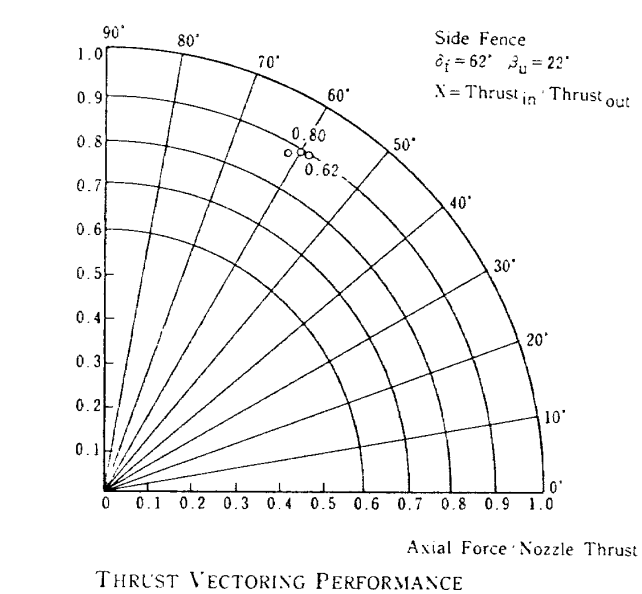

Figure 21 Thrust vectoring performances for flap setting δ_f = 62°, USB nozzle kickdown angle of 22°.

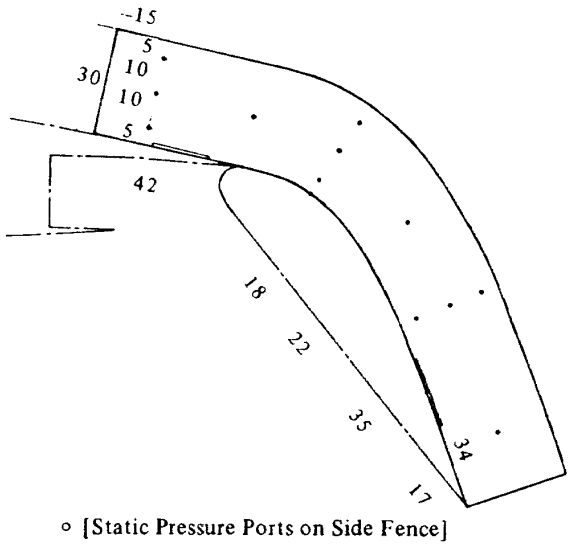

○ [Static Pressure Ports on Side Fence]

Figure 23 Locations of static pressure ports on Side Fence

smaller portions. These tendencies were quite reasonable because a higher kickdowned USB nozzle brought the exhaust jet flow spreading outwardly so that its wall jet thickness became thinner which enhanced the Coanda parameter and the side fence tended to play a lesser role.

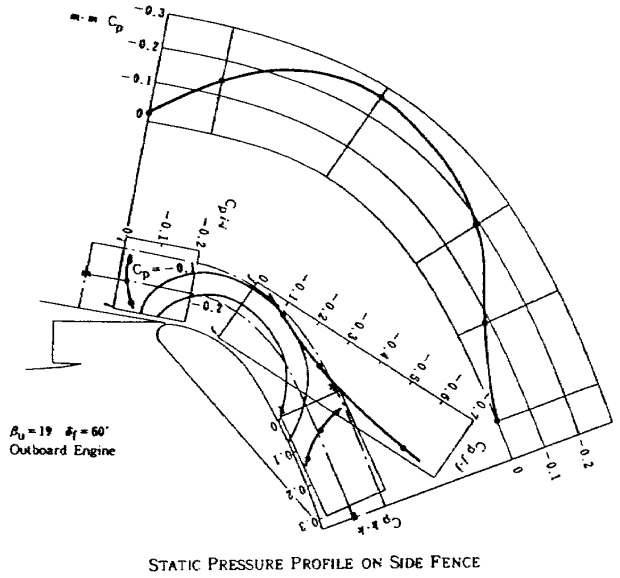

Figure 24 C_p profiles on Side Fence for $\delta f = 60°$, $\beta u = 19°$ Outboard engine side

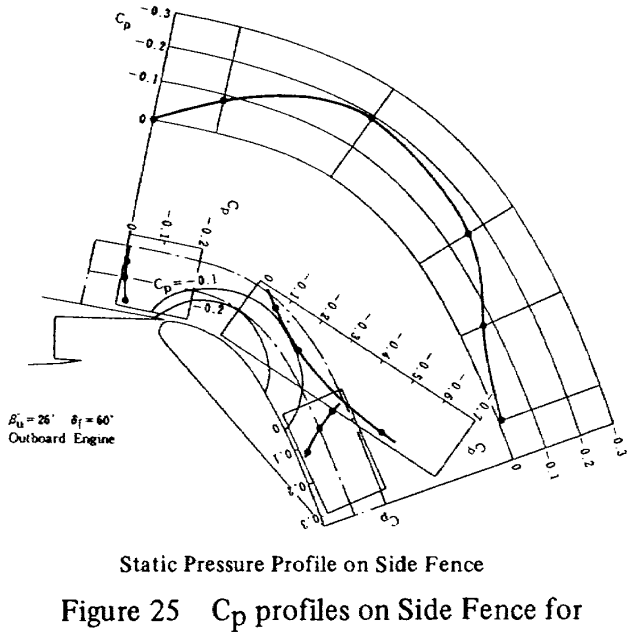

Figure 25 C_p profiles on Side Fence for $\delta f = 60°$, $\beta u = 26°$ configuration. Outboard engine side

WIND TUNNEL EXPERIMENT

A research program has been undertaken at the National Aerospace Laboratory [NAL] to determine the effect of side fences on the powered lift aerodynamic characteristics of a four-engine USB configuration. The 8%-scale semispan model used in this study simulates the NAL Quiet STOL Research Aircraft (cf. Figure 26) which has a nominal quarter-chord wing sweep back angle of 20°. The inboard and outboard engine nacelles are located at 23.8 percent (Wing station, WSTA=92) and 79.2 percent (WSTA=306) of USB flap span (385.8

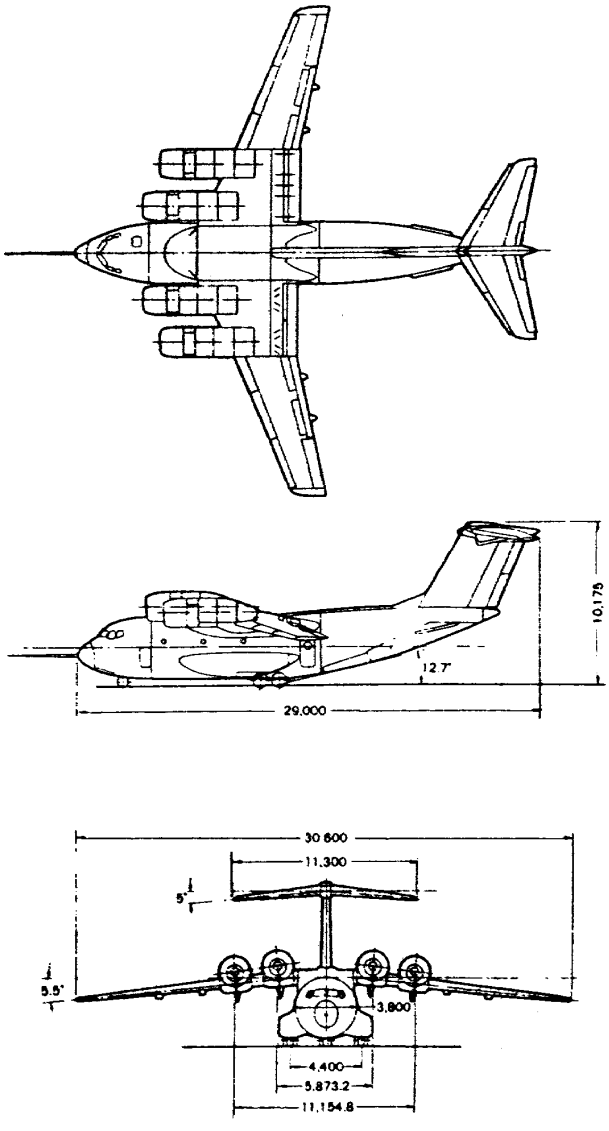

Figure 26 General View of NAL Quiet STOL Research Aircraft

mm), and 40.0 and 36.6 percent of wing chord respectively.

Simulator engines equipped with D-shaped exhaust nozzles (AR_e=2.63, β_u=19°) were supplied with high pressure air from the fuselage and control valves to permit simulation of the exhaust flow characteristics of turbofan engines.

A photograph of the wind-tunnel installation for the basic model configuration is presented in Figure 27-(1),(2).

The engine static thrust calibrations to determine the thrust as a function of engine reference pressure were carried out prior to testing with the engines installed on the half-model and with the USB flaps and the main wing trailing edge plates removed. The static thrust was computed as the resultant of the normal and the axial forces.

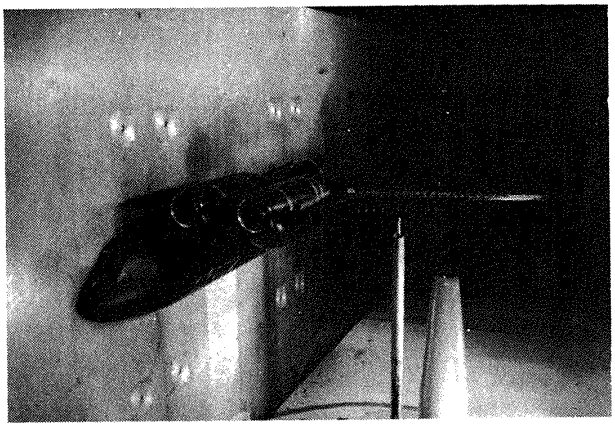

Figure 27 – (1) A photograph of the wind tunnel installation for a basic model configuration.

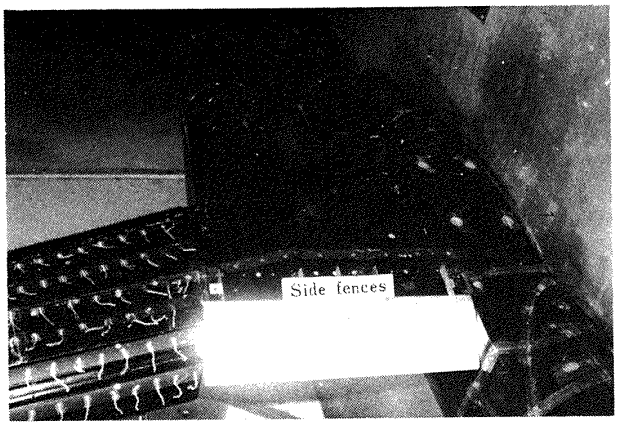

Figure 27 – (2) Basic model configuration with side fences installed.

The thrust coefficients C_j stated in nomenclature for the wind-on aerodynamic tests were determined from the summation of the static thrust of the inboard and outboard engines based on the engine reference pressure recorded at wind-on data points.

The tests wre conducted with the horizontal tail removed. The static performances were measured at an angle of attack of 0° for the USB flap configuration, δ_f=60°. Wind-on aerodynamic tests were conducted with several values of thrust coefficients C_j which were held constant as the angle of attack α was varied through an range of −10° to approximately 35°. Aileron and Wing leading edge boundary layer controls were incorporated to delay the wing stall to attain higher maximum lift.

The locations of the five side fences installed are at WSTA=40, 147, 200, 254, and 360 respectively. The height of the side fence is 15 mm which is approximately 30 percent of the maximum height of D-shaped USB nozzle, h.

Figure 28 shows the effect of side fences on static jet turning performance for the USB flap configuration, δ_f=60°, compared with the typical deployment of vortex generators (with an incidence angle of 30° and an aspect ratio [chord to span] of 2.5). The results are presented in terms of the jet turning angle δ_j as functions of

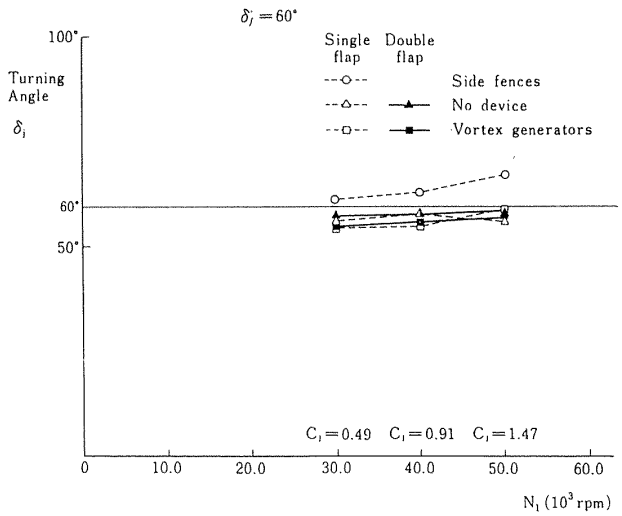

Figure 28 Effect of side fences on the jet turning performance

the simulator engine's fan rotor speed N_1. The installation of side fences provides about 10° improvement. Also values of the jet turning angle δ_j tend to increase with increasing fan rotor speed, except for the configuration using no special devices.

Figure 29 presents the customary polar plot

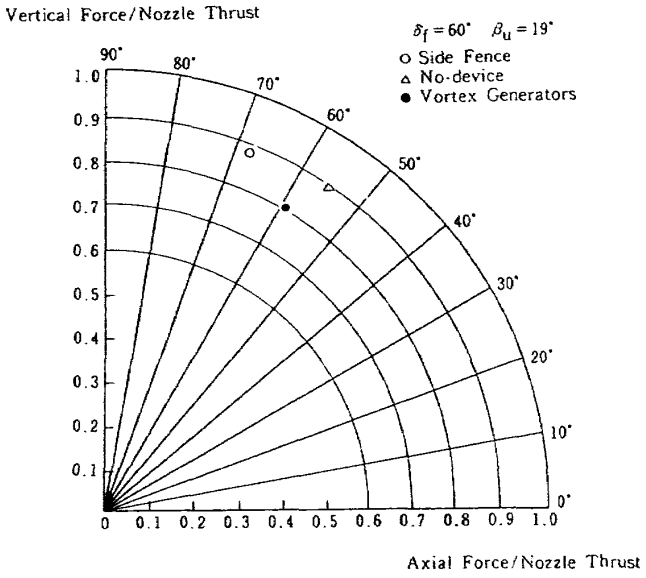

Figure 29 Thrust vectoring performace

which summarizes the thrust vectoring performance at fan rotor speed N_1=50000 rpm. The USB configuration with side fences achieves higher jet turning efficiency (η_j=0.89) compared with vortex generators (η_j=0.80). The results are quite consistent with the preliminary static data.

The aerodynamic characteristics for the corresponding USB flap configuration in the low-speed wind tunnel experiment (U_∞=30m/s) as a plot of the lift coefficient C_L and the drag coefficient C_D against the angle of attack α are presented in Figure 30 and 31 respectively. The data are shown for the thrust coefficient C_j=0.49, 0.91 and 1.47. For the thrust coefficient C_j=1.47, a maximum lift coefficient was 6.62 (side fences), whereas the power-off maximum lift coefficient was about 2.2. The dramatic improvement in lift characteristics by the installation of side fences is shown in Figure 30. Also, side fences achieved a lift performance superior to vortex generators; i.e., an increase in both maximum lift coefficient C_{Lmax} and stall angle of attack can be seen. The wing stall occurred beyond approximately 19° of attack angle for

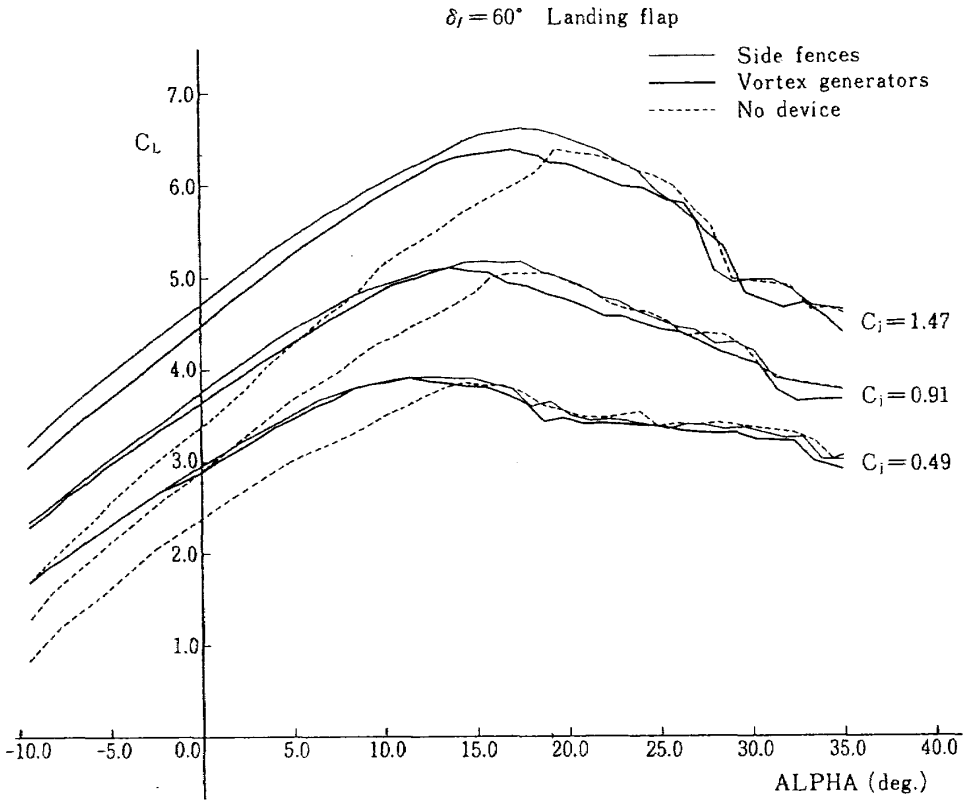

Figure 30 Effect of side fences on lift characteristics ($\delta_f = 60°, \beta_u = 19°$)

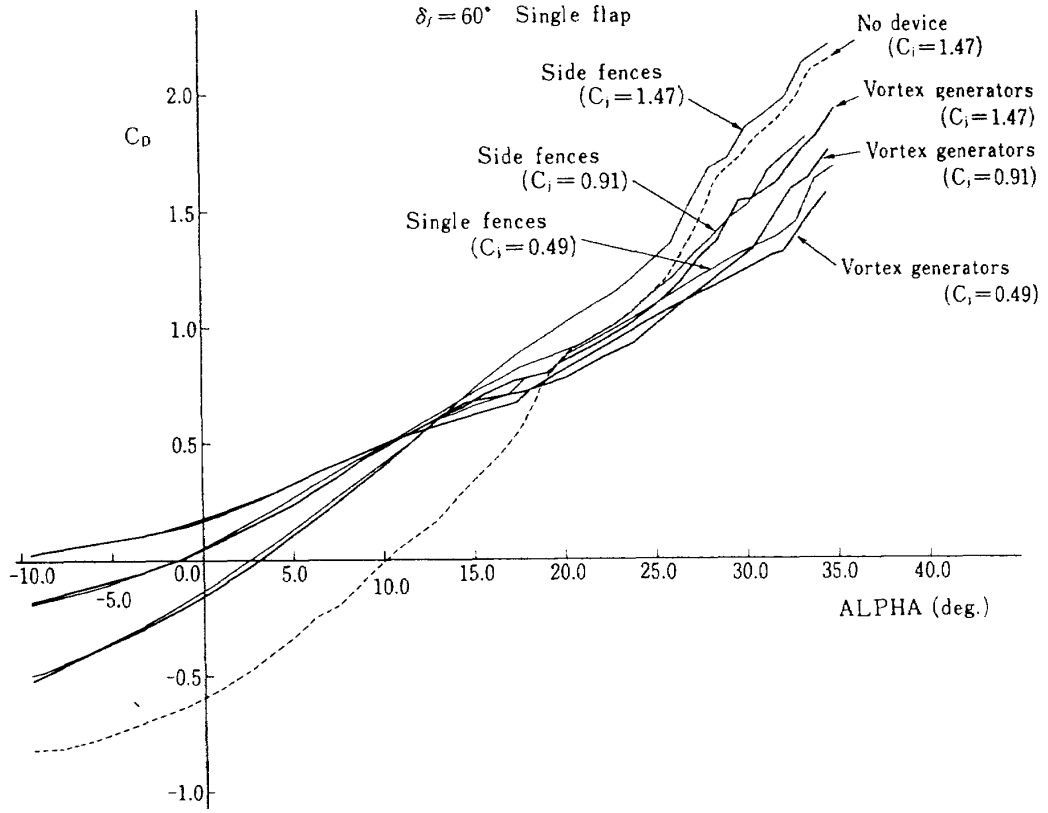

Figure 31 Effect of side fences on drag characteristics ($\delta f = 60°$, $\beta u = 19°$)

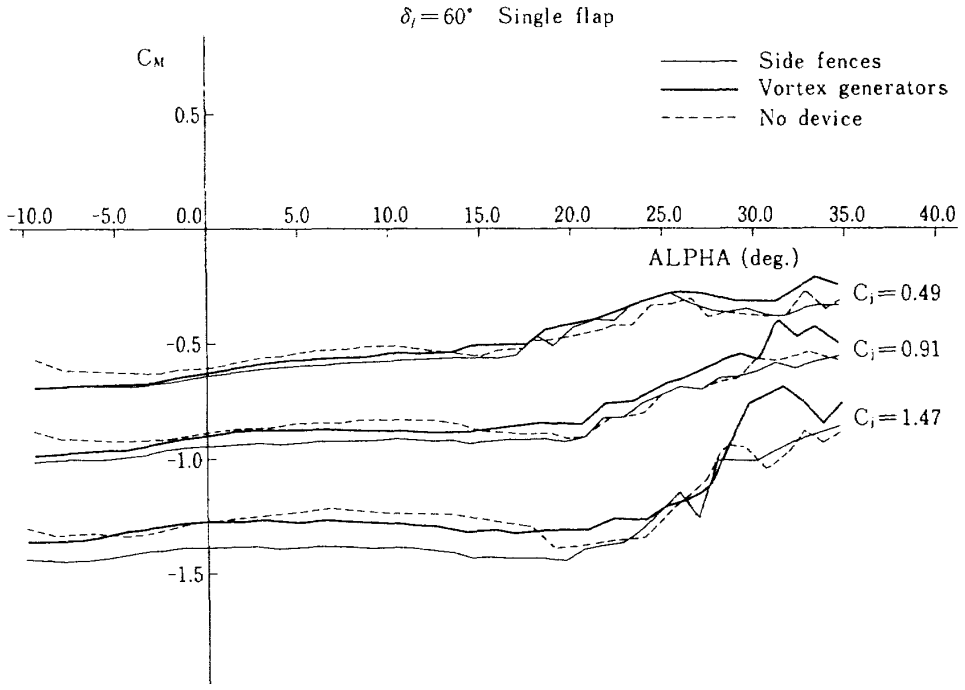

Figure 32 Effect of side fences on pitching moment coefficient ($\delta f = 60°$, $\beta u = 19°$)

the thrust coefficient C_j=1.47 with side fences configuration (16° of attack angle with vortex generators), accompanying sudden increase of drag coefficients. As indicated in Figure 31, side fences induced considerable drag, compared with vortex generators, in the high angle of attack range for the USB flap configuration, δ_f=60°.

Figure 32 presents the pitching moment coefficient C_M against angle of attack α for the landing flap configuration with the horizontal tail off. As indicated in the pitching moment plots, the USB configuration with side fences paid a slight penalty for its superior lift performance; i.e., higher negative pitching moments were observed compared with vortex generators. In view of the results indicated in C_p profiles and their contours on the inner surface of the side fence presented in Figures 24 and 25, it is possible, by tailoring the side fences, to further reduce the size of side fences without deteriorat-

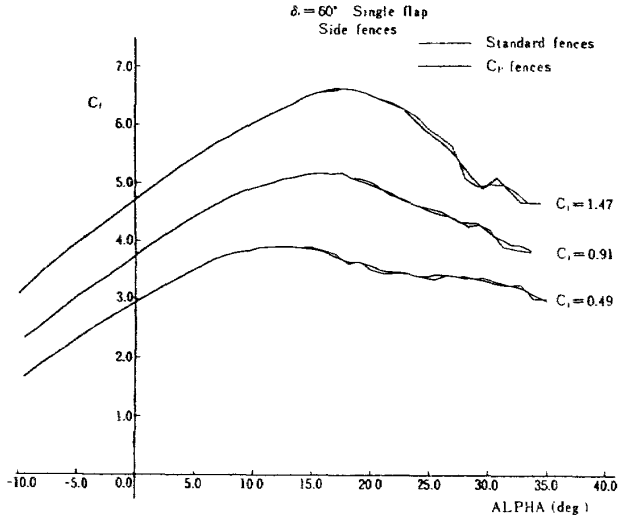

Figure 33 Comparison of standard side fences and C_p fences in lift characteristics

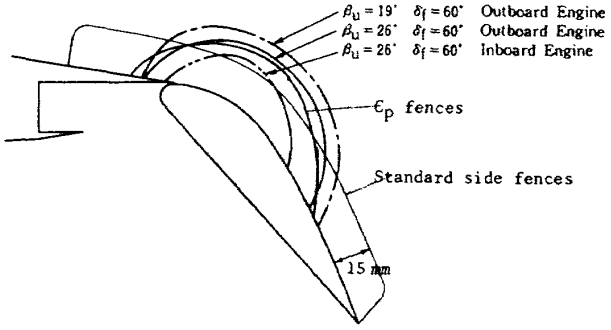

[STATIC PRESSURE CONTOUR (C_p=−0.1) ON SIDE FENCE]

Figure 34 Geometry of C_p fences

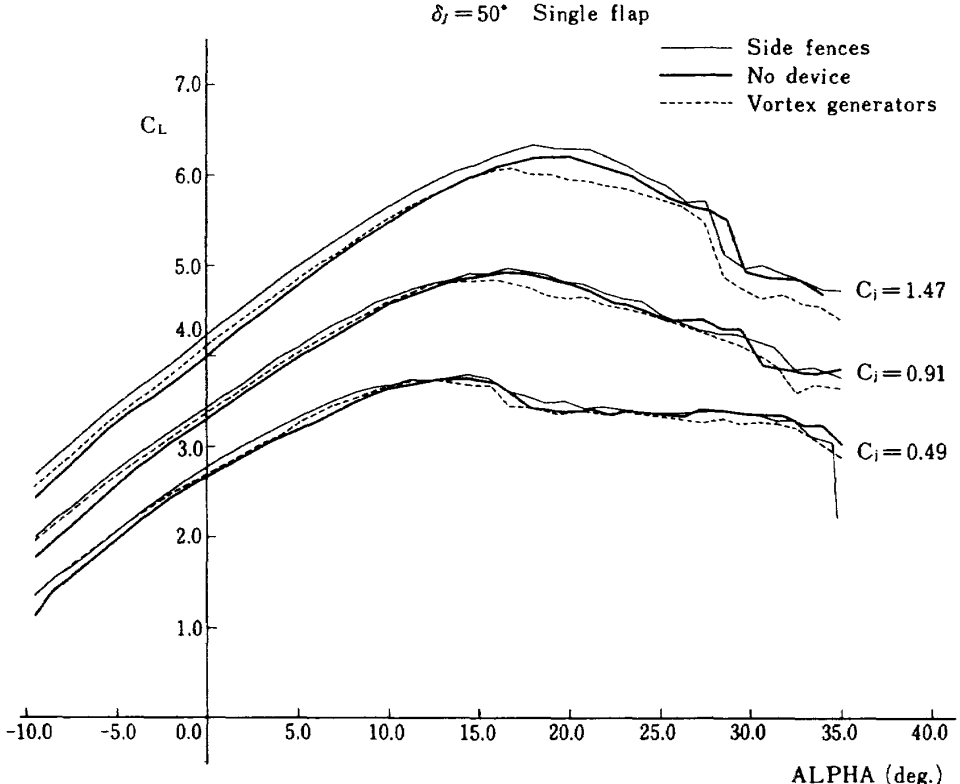

Figure 35 The lift coefficient for the landing flap configuration δ_f= 50°

ing their performances. Figure 33 presents the comparison of standard side fences add C_p fences (cf. Figure 34) in lift characteristics.

Figure 35 presents the lift characteristics for the landing USB flap configuration $\delta f=50°$, where the configuration without any special devices attains comparable lift coefficients to those attained by the configuration with vortex generators installed. In Figure 36, the lift characteristics of 40° USB double (fore/main) flap configuration without any special devices are compared with those of vortex generators. For such the low flap setting configuration as double flap $\delta f=40$, it may be of no use to install the flow attachment device like vortex generators.

The lift-drag polars for the landing flap configuration $\delta f=60°$ as shown in Figure 37 indicates that configurations using either side fences or vortex generators have the positive drag necessary for descent in the required high lift range. Based upon the untrimmed C_L/C_D data of

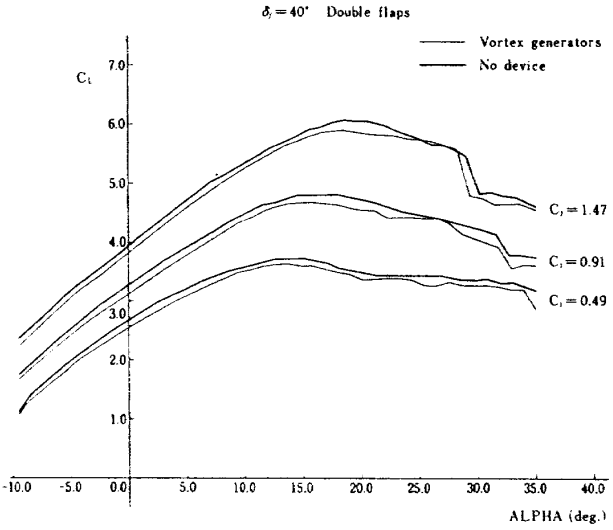

Figure 36 The lift coefficient for the USB double flap configuration $\delta f = 40°$

Figure 37, the landing configuration with side fences installed has better descent capability than with vortex generators, for example, with the flight path angle $\gamma=-8°$ and the thrust coeffi-

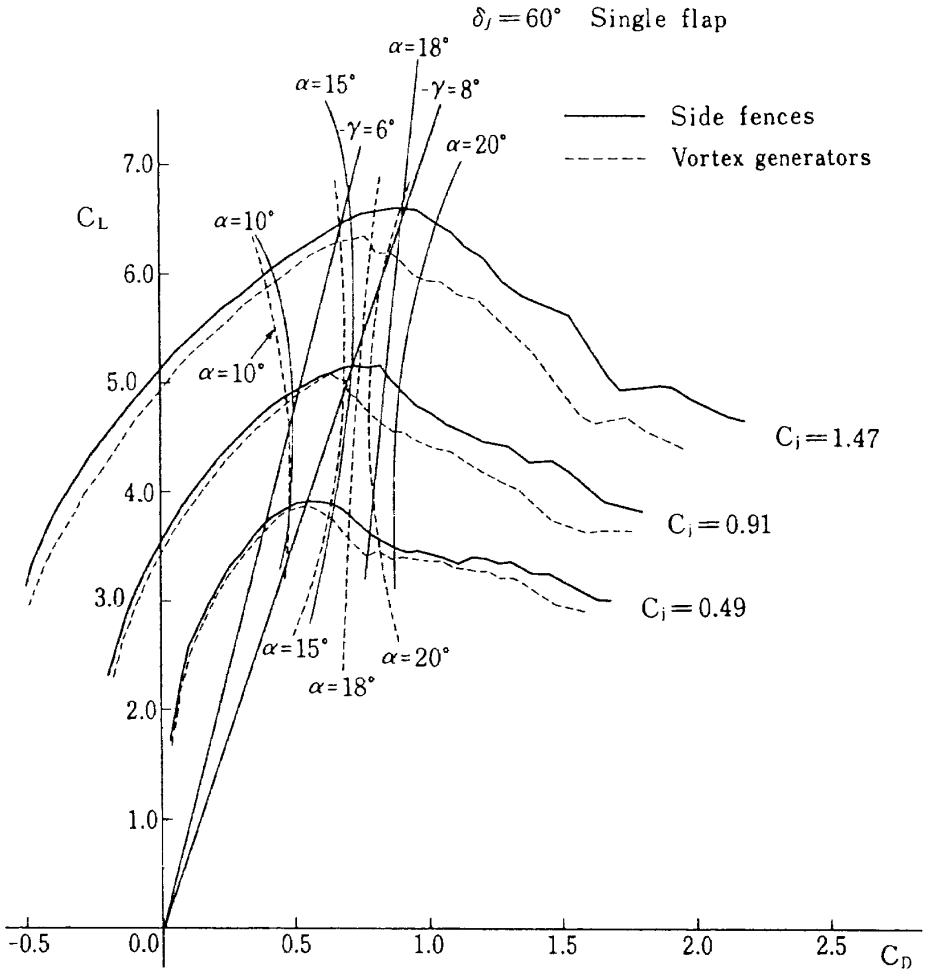

Figure 37 Lift-drag polars for the landing flap configuration

cient C_j=0.91, side fences achieved C_L=5.2 at the angle of attack α=15°, while in order to arrest this descent at the same flap setting with the same thrust in a configuration using vortex generators, the required approach angle of attack goes beyond the stall angle of this configuration with a decrease in C_L(=4.8).

CONCLUDING REMARKS

The fundamental aspects concerning the effect of side fences on powered lift augmentation for the external upper surface blowing propulsive-lift configuration, as ascertained by wind tunnel experiment using the 8%-scale semispan model of NAL Quiet STOL Research Aircraft, were presented.

From the comparisons we have made of configurations using side fences, those using vortex generators and those without any special devices, we conclude that the USB propulsive-lift concept using side fences for enhancement of engine exhaust flow attachment has promising potential for attaining high and efficient powered lift performances. It should be emphasized that the preceding comparisons are mainly based upon data of lift-drag and longitudinal aerodynamic characteristics, and wind tunnel studies are to be further continued to obtain data such as lateral or trim characteristics required for more detailed quantitative performance comparisons.

ACKNOWLEDGEMENT

This research was carried out as a part of the Research Project of Fan-Jet STOL Aircraft. The author would like to express sincere thanks to the Division Directors, Mr. Tadao Torisaki and Dr. Masakatsu Matsuki for their valuable advice and comments. The author is also indebted to Mr. Kenichi Hirosue and Mr. Akihito Iwasaki of V/STOL Aircraft Group for their helps in carrying out the experiments.

REFERENCES

1. Braden, J.A. et.al., "Cruise Aerodynamics of USB Nacelle/wing Geometric Variations." NASA SP-406, 1976.
2. Grotz, C.A., "Development of the YC-14 Propulsion System." AIAA Paper 75-1314, 1975.
   Hirt, W.J. et.al., "Method of and Apparatus for Enhancing Coanda Flow Attachment Over a Wing and Flap Surface." United States Patent 4019696.
3. Maita, M. et.al., "Acoustic Characteristics of the External Upper Surface Blowing Propulsive-Lift Configuration."
   AIAA Paper 80-1063 and Journal of Aircraft, Vol.18, No.8, 1981.
   Maita, M. et.al., "Development of USB Propulsive-Lift Device."
   AIAA Paper 80-1244, 1980.

TECHNICAL REPORT OF NATIONAL
AEROSPACE LABORATORY
TR-686T

航空宇宙技術研究所報告686T号（欧文）

昭和56年10月発行

発行所　航空宇宙技術研究所
東京都調布市深大寺町1880
電話武蔵野三鷹(0422)47-5911(大代表) 〒182
印刷所　株式会社　共進
東京都杉並区久我山5－6－17

Published by
NATIONAL AEROSPACE LABORATORY
1,880 Jindaiji, Chōfu, Tokyo
JAPAN